COBEM 2023 27TH INTERNATIONAL CONGRESS OF MECHANICAL ENGINEERING

ABCM Brazilian Society of Mechanical Sciences and Engineering
27th ABCM International Congress of Mechanical Engineering
December 04-08, 2023, Florianópolis-SC, Brazil

COB-2023-0090
Numerical Analysis of the Blade and Tower Aerodynamics of the NREL 5MW Wind Tower Project.

Vinícius Massoni Pires
Reginaldo Ribeiro Sousa
Bruno Moreira
Augusto Salomão Bornschlegell
Universidade Federal da Grande Dourados; Rodovia Dourados-Itahum, Km 12 - Cidade Universitária- FAEN, Dourados, Mato Grosso do Sul, Brasil
vinicius.pires058@academico.ufgd.edu.br, augustosalomao@ufgd.edu.br

Abstract. *Wind turbines has increasingly been studied in order to provide technical solutions to the challenges in converting eolian energy into electricity. Among these different challenges, the blades' aerodynamics has to be optimized and data related to these geometries are normally confidential. The NREL 5 MW project is a available study case (i.e. a benchmark) with detailed information about the blade geometry. As the blade rotates, a control system adjust the blade's angle of attack in order to maximize energy conversion as well as to avoid overload to its structure. When the blade's tip is at the lowest point, the blade is aligned with the tower. Thus, the blade aerodynamics may experience a different behavior. In this work, we evaluate flow behavior or the NREL blade when it is far away from the tower and when it is just in front of the tower. To attain this task, o numerical 2D model, covering the blade mid plane cross section, was developed. We used the pisoFoam solver from OpenFOAM v8. The numerical schemes employed were backward second order for time integration, upwind second order for the advective terms treatment and PISO algorithm for the pressure-velocity coupling. As boundary conditions, the velocity of 20 m/s is imposed at the inlet and the slip condition at the top and bottom limits. These configuration led to Reynolds Number of 9.6x104. At the blade and tower surfaces, the non-slip boundary condition was applied. The domain discretization was performed with the blockMesh and snappHexMesh solvers from OpenFoam. The GCI method was employed to verify the results sensibility to the mesh. The final mesh has 430 k cells, which 426 k are hexahedra and 4 k are polyhedra (3.4 k with 7 faces and 0.6 k with 8 faces). The standard values of the aerodynamic coefficients are in good agreement with the results obtained with the proposed model. The results regarding the blade far from the tower (case A) and the blade in from of the tower (case B) can be summarized as follows. The flow behavior in case A is stead whereas in case B, it presents a sinusoidal behavior at 2 Hz. The aerodynamic forces was increased by 25% in magnitude in case B. Then, we could conclude that the presence of the tower affects not only the aerodynamic forces magnitude, but also its behavior over time.*

Keywords: *Wind Turbine, CFD simulation using OpenFoam, Grid convergence Index GCI, NREL 5 MW.*

1. INTRODUCTION

In recent years, a panorama can be seen where electrical energy is and will be increasingly used. The current energy sources that dominate the planet, despite supplying the demand, are mostly non-renewable. According to the International Energy Agency (Bojek, 2022), from the world energy matrices, only 2% are renewable energies, while 31.1% belong to oil and its derivatives, 23% to gas reserves natural and 27% to mineral coal. Other different energy sources corresponds to the remainig 16%. In the national scenario, according to the National Energy Balance (EPE, 2021), about 7.7% of the Brazilian energy matrix used in the country is renewable. The highest percentages belong, respectively, to Oil and derivatives (33.1%), sugarcane and derivatives (19.1%), hydraulics (12.6%) and natural gas (11.8%).

In the case of the World Electricity Matrix, the outlook is more encouraging; 8.2% (Bojek, 2022) of the matrix are renewable, while coal (36.8%), natural gas (23.5%) and hydraulic sources (16.1%) dominate the scenario . In Brazil, the electrical matrix is more renewable than the energy matrix on a large scale, where only wind energy, the main theme addressed in this work, represents 11% (EPE, 2021) of the matrix, followed by the increase in solar energy in recent years, where there was a 50% increase in demand during the Covid-19 pandemic (ABSOLAR, 2021). Most of the matrix is still concentrated in hydroelectric plants, with 65.2% of the energy matrix.

In fact, the potential of renewable energy generation tends to grow according to the use of non-renewable energy, given the technological expansion that the potential for use in operation at lower consumption of non-renewable energy. Wind energy is shown to be fundamental in this role; in 2020, according to the IEA (Bojek, 2022), wind energy growth (compared to 2019) increased by 144 Twh, about 11% higher. China and the United States are the two biggest countries in energy growth, followed by the European Union, India and Brazil.

With regard to Brazil, between the year 2011 and January 2022, the country showed an increase from 1 GW installed to 21 GW (Brasileiro, 2021), and came to occupy the sixth (6th) place in Total Installed Capacity of Onshore Wind Power in 2021, according to the Global Wind Energy Council (GWEC, 2021). In addition, a ten-year energy plan (PDE 2031) was launched with the expectation that the installed capacity of national electricity generation will reach a level of renewability of approximately 83% (Brasileiro, 2021).

Considering the proportion and expectations about the growth of wind energy, it is necessary to be in constant improvement and innovation to provide greater safety and performance. New areas such as the maritime and also large urban centers were conceived as turbine centers. However, the concern with the fauna and the efficiency of energy production must be as well as the search for renewal.

1.1 RELATED WORK

The authors in Santoni *et al.* (2017) described the behavior of the tower and nacelle in the part of the fluid wake passing through the turbine as a whole. Computational fluid dynamics (CFD) simulations were performed in ALM software, using the Navier-Stokes and continuity equations to calculate the flow. Large Eddy Simulations (LES) was used by the authors to model the turbulent flow. The domain used was a three-dimensional model with dimensions of 1.1 x 0.26 x 0.18 m. For the simulations, two and three-dimensional models were used using only the blade and later the entire structure in the mesh.

The results from Santoni *et al.* (2017) compares two geometrical models at the wind speed of 10 m/s. The first model does not represent the nacelle and the tower whereas the second model does. Without the nacelle, the wind speed has increased by 1.15 from its initial value, in addition to the non-physical jet behavior in the center of the rotor. The maximum speed was maintained for about 0.25 meters behind the rotor, followed by further flow dissipation as it aproaches to the opposite (outlet) boundary condition.

Considering the rotor and nacelle, it has been observed a moment deficit that is not aligned with the flow direction. This is due to the direction of the fluid after contact with the nacelle and blade is changed a few degrees downwards, as a result of the drop in speed. When all the elements are modeled, it is also possible to notice a momentum about 40% smaller compared to the previous cases in the lower part of the tower. Not least, the authors also notice a recicurlation zone at the rear of the tower in the simulations, its size being related to the size of the tower and decreasing with the proximity of the nacelle.

1.2 Objective

The objective of this work is to analyze the behavior of the aerodynamic coefficients of the midplane section of the blade profile and the tower of a wind turbine when the blade is positioned in front of the tower, as illustrated in Fig. 1. The software used will be *OpenFoam*, in version 8.1.

2. METODOLOGY

2.1 Mathematical Model

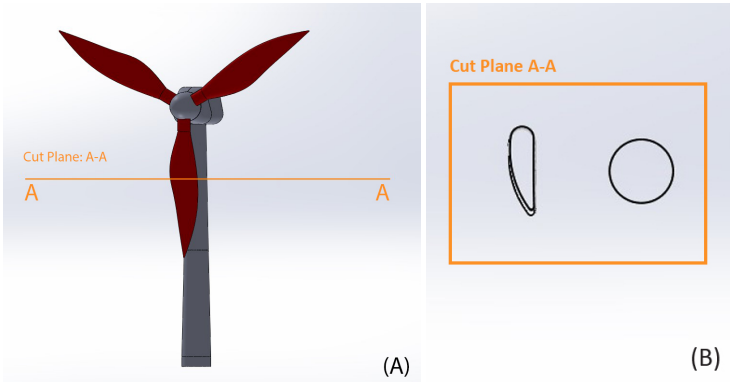

Figure 1. (A) Wind Turbine Model; (B) Sectioned Plane and Resulting Geometry

The midplane blade profile is the DU25-A17, which presents a twist angle of 7° in relation to the origin (vertical, upright). The blade was divided into 17 elements, and the element studied will be the number 8. The data found refer to values between the angles of 90°and 85°, values listed by NREL (Jonkman *et al.*, 2009). The properties of the profile used in the modeling are as presented in Table 1.

Table 1. Profile and Tower Input Data

Variable	Initials	Value	Unit
Tower Diameter	D_t	0.0396579	m
Cord length	D_w	0,01002848	m
Profile Thickness	E_p	0.005	m
Profile Area	A_p	0.00019829	m

The numerical model is then a reduced scale of the original model by 1:100. The scale was used to adapt to the wind tunnel parameters present in the laboratory. The DU25-A17 profile will be analysed with and without the tower behind it. The tower section used in the simulation (section on the same level as the profile is located) has a diameter of $0.0396579\ m$ and is positioned just behind the blade profile, at a distance of $0.0023\ m$.

The Navier-Stokes equations are used to describe the flow behavior. For the case studied, the flow was modeled using the Reynolds Average Navier Stokes (RANS) (Alfonsi, 2009). The average Reynolds models are based on the decomposition of velocity into an average value and intermediate fluctuations.

The study was carried out following the transient flow regime with constant properties, listed in Table 2, the following input conditions were used;

Table 2. Input Data from the case

Variable	Initials	Value	Unit
Wind Speed	V	20	m/s
Air Density	ρ	1.225	$\frac{kg}{m^3}$
Dynamic Viscosity	ν	1.10^{-5}	$\frac{kg}{m.s}$
Turbulent Intensity	I	5	$\%$

The speed was based on NREL (Jonkman *et al.*, 2009) standards as a reference for the blade and wind turbine model. The density of follows the IUPAC standard values. Two cases will be presented for the constant properties; one with only the blade being analyzed in the mesh; another with the blade and the tower together in the same analysis, both using the previously mentioned boundary conditions.

2.2 Nondimensional Parameters

For the present study, the knowledge about the flow phenomenon around the bodies and its variations according to the type of fluid and changes caused by external agents is of paramount importance; when a body is in contact with a fluid and there is movement between them, two force components appear, called drag force (F_d) parallel to the flow direction and lift force (F_l), perpendicular to the flow. It is important to note that the study was carried out with a simplified two-dimensional analysis. In this way, forces are considered per unit length in the axis direction.

$$C_D = \frac{2 \cdot F_d}{\rho \cdot AV^2} \tag{1}$$

$$C_F = \frac{2 \cdot F_f}{\rho \cdot AV^2} \tag{2}$$

where C_D represents the drag force value, C_F represents the lift force value, ρ is the fluid density, in the case of air and V the velocity value. F_d and F_c are drag and lift forces, respectively.

When in contact with the cylindrical body, the fluid generates what is called the region of disturbed flow. It is sensitive to small variations in flow and the Reynolds Number (R_e). The deal will present a high Reynolds Number, considering the flow as turbulent; [10]

$$R_e = \frac{V \cdot D}{\nu} \tag{3}$$

Where V is the velocity value, D the length of the adopted body, and ν the kinematic viscosity of the fluid in question.

2.3 Numerical Model

Regarding the mesh, it has 3 dimensions, however, as only the x and y components will be analyzed, the third component was used with only one element. The mesh has a size of 274 volumes in x, 127 volumes in y and 1 volume in z thought to have the characteristic dimensions of the experimental wind tunnel. The discretization is illustrated in Fig.2. As the problem was modified to be two-dimensional, the unit in z has a minimum unit value in order not to present variations in the result.

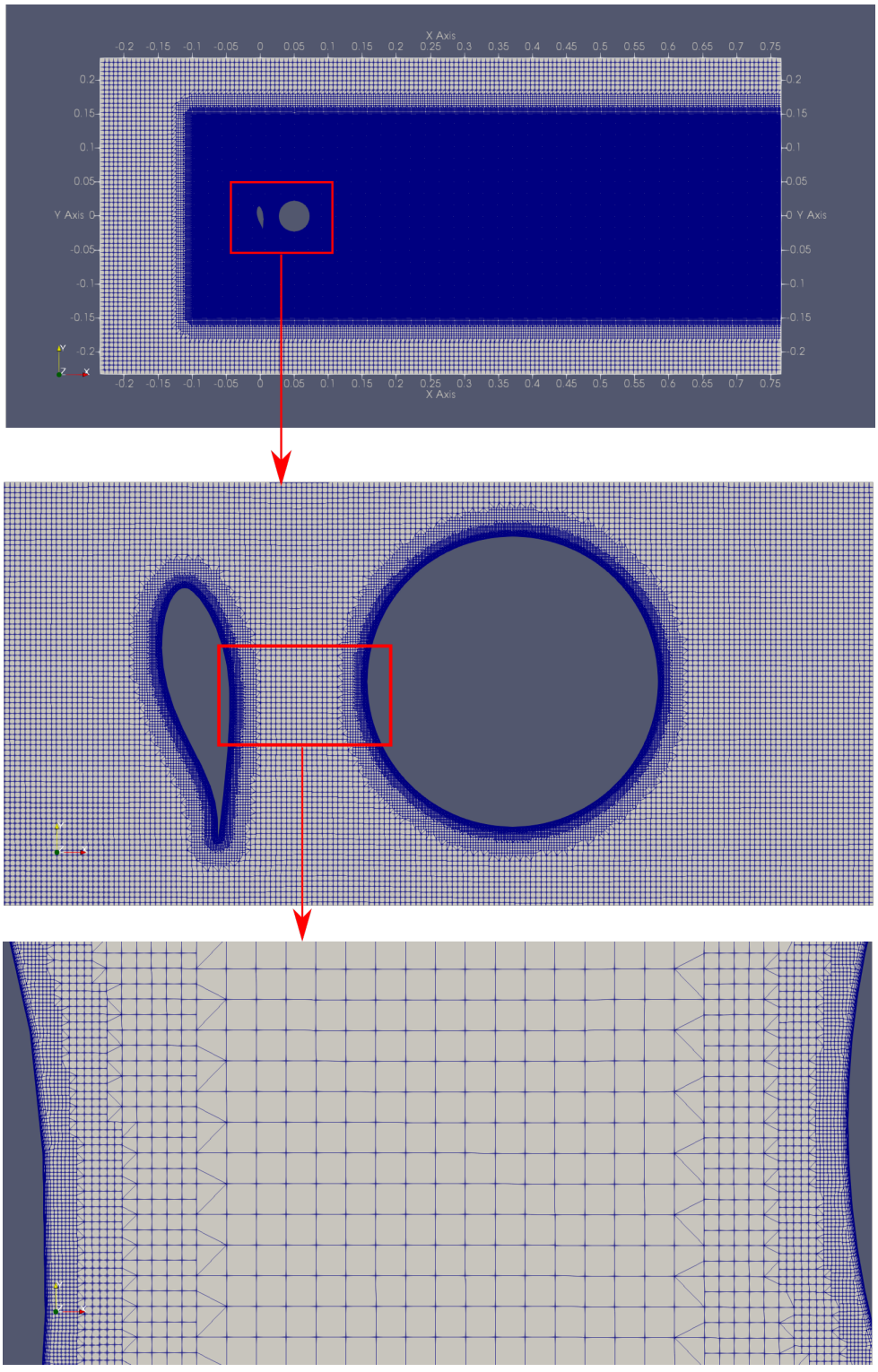

Figure 2. Domain discretization

With regard to the divisions of the mesh, in order to obtain a result that is more consistent with the possible reality,

it was divided into four main boundaries; *inlet*, representing the part with the input data, *profile*, *tower*, representing respectively the areas of the blade and tower profile in the mesh and *outlet*, with the data output of the problem. In addition, there are the patches *top* and *bottom*, which represent the upper and lower walls of the mesh.

For the numerical analysis, the turbulence model was the k-omega Shear Stress Transport (SST) (Menter, 2003), which is a two-equation model, one for the turbulence kinetic energy (k), and another for turbulence specific dissipation rate (ω). The fluid regime is transient, using the Backward Facing Step (BFS) second order model [OpenCFD (2018)] together with the pressure-velocity coupling (PISO) solver (Ferziger *et al.*, 2002). The treatment of advective terms used was upwind, also in second order (Spalding, 1972).

Table 3. Properties calculated for turbulent flow

Variable	Initials	Value	Unit
Turbulent Kinetic Energy	K	1.5	$\frac{J}{kg}$
Specific Turbulent Dissipation	ω	612.37	$\frac{1}{s}$
Turbulent Dissipation	ϵ	82.670	$\frac{J}{kg.s}$
Reynolds Number	Re	$9.60\text{x}10^4$	Nondimentional

Based on the input data, the turbulence variables calculated are presented in Table 3, are necessary for the simulation settings via *OpenFoam*. To perform the calculations, the *CFD Tool* (CFDOnline, 1998) was used, a tool for calculating turbulent properties and estimates.

The simulation will be carried out in a two-dimensional model due to the processing capacity of the simulations.

3. RESULTS

3.1 Mesh Independence Test

For comparison and refinement methods, three meshes with different numbers of cells were used, listed in the table 4. The mesh 1 is the finner mesh with 748 k cells and mesh 3 is the coarsest with 246 k cells. To perform a discretization estimation calculation, it is recommended to calculate the factor called h which can be found by dividing the total area of the mesh by the total number of cells. This value needs to be greater than 1.3 (Celik, 2008) to set the mesh to fine. Thus, with the given values we have a factor with a value of 1.32 (Celik, 2008).

$$h = \left[\frac{1}{N} \sum_{i=1}^{N} \Delta A_i \right]^2 \tag{4}$$

Then an iterative method is used to compare the meshes, as follows:

$$p = \frac{1}{ln(r_{21})} \cdot \left| ln \frac{\epsilon_{32}}{(\epsilon_{21})} + q(p) \right| \tag{5}$$

$$p(q) = ln \left(\frac{r_{21}^p - s}{r_{32}^p - s} \right) \tag{6}$$

$$s = 1 \cdot sgn \left(\frac{\epsilon_{32}}{\epsilon_{21}} \right) \tag{7}$$

Where p is the variable for ordering the method, ϵ_{32} and ϵ_{21} are variables used to compare the meshes, using a representative data of the problem (Celik, 2008). For the current work, the data used will be the drag force between the meshes, as follows:

$$\epsilon_{21} = F_{d1} - F_{d2} \tag{8}$$

$$\epsilon_{32} = F_{d2} - F_{d3} \tag{9}$$

The variables r_{21} and r_{32} are the ratios between the refinement factors of the respective h meshes (Celik, 2008). The values with the comparisons between the refinements of the three meshes presented.

$$r_{21} = \frac{h2}{h1} \tag{10}$$

$$r_{32} = \frac{h3}{h2} \tag{11}$$

To calculate the independence test, using the parameters mentioned above, the following formula is used (Celik, 2008);

$$GCI_{2,1} = \frac{1.25 e_a^{2,1}}{r_{21}^p - 1} \tag{12}$$

Where $e^{2,1}$ is the error estimate calculation containing the values of ϵ. ϕ can be calculated by the equation 14:

$$e_a^{21} = \left| \frac{\phi_1 - \phi_2}{\phi_1} \right| \tag{13}$$

$$\phi^{21} = \left(\frac{r_{21}^p \cdot \phi_1 - \phi_2}{r_{21}^p - 1} \right) \tag{14}$$

In the same way, ϕ_{32} is calculated

Table 4. Mesh Comparsion

Mesh	No. cells	F_d	r_{xy}	C_d
1	748.324	0.06841	1.3247	1.7250
2	430.932	0.06951	1.3177	1.7529
3	246.415	0.08892	1.3224	1.8304

Table 5. CGI Results for Each Mesh

Comparation	CGI
1-2	1.1193
2-3	3.0093

The value of F_d presented in the Table 4 represents the average value of the force acting over the blade for the presented flow. From the meshes used, it is noticed a convergence in the value of F_d in the meshes 1 and 2, as presented in Table 5. The value of the drag force presents similar values in the meshes 1 and 2, in addition to a result also close to the mesh number 2. Thus, the selected mesh for our analsis is the Mesh 2.

3.2 Blade

Given the input and output parameters, in addition to the mesh used, for a time interval of 20 seconds, the following results were obtained for the drag and lift coefficient.

Observing the behavior of the blade over time, it is possible to identify a large variation at the beginning of the simulation, over the initial 8 seconds. This variation can be explained by the first contact with the angulation of the blade profile used, of 83°, causing high fluctuations in both the drag coefficient and the lift coefficient. The input velocity of 20 m/s generates a detachment of the boundary layer after contact with the profile.

As presented in Fig. 3, a stable result is analyzed, with a drag coefficient around $1.6 - 1.7$ and lift coefficient around $0.4 - 0.5$ for a Reynolds Number of $0.96\text{x}10^5$. It is important to note that both C_l and C_d variations occur simultaneously. Comparing the numerical results obtained with the NREL (Jonkman *et al.*, 2009), both the values found in the present work are 0.2 higher, but the Reynolds Number, used for the NREL experiments was $0.75\text{x}10^6$ (Jonkman, 2016).

Regarding velocity (Fig. 4), the sharp drop in velocity observed at the rear of the profile is due to the angle which it is located, also resulting in a speed drop value of approx 90% regarding to the beginning of the shearing layer. A pattern increase in velocity can be observed at the leading and trailing edge exits of the profile, resulting in the boundar layer deattachment from the blade profile, as shown in the image. In this way it is possible to understand the time for convergence of the drag and lift results, given the large recirculation zone left at the rear of the profile.

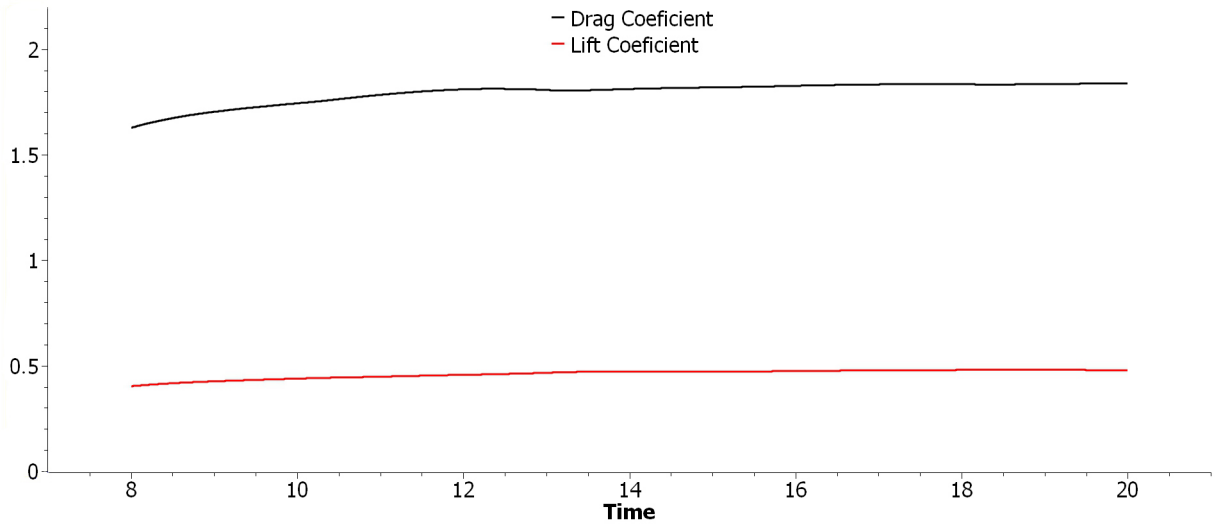

Figure 3. C_l and C_d Values Over Time

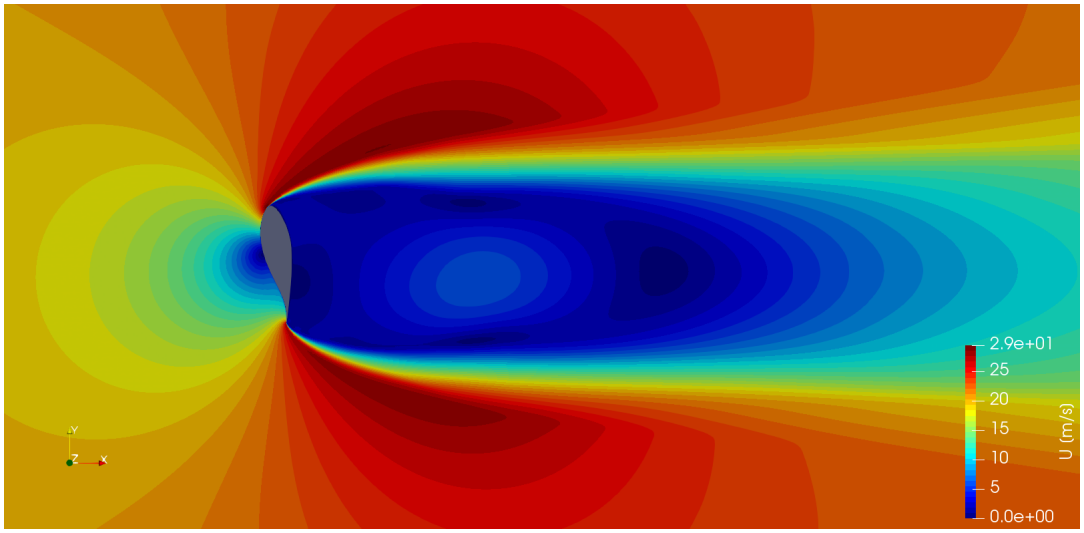

Figure 4. Velocity field at $t = 20\ s$

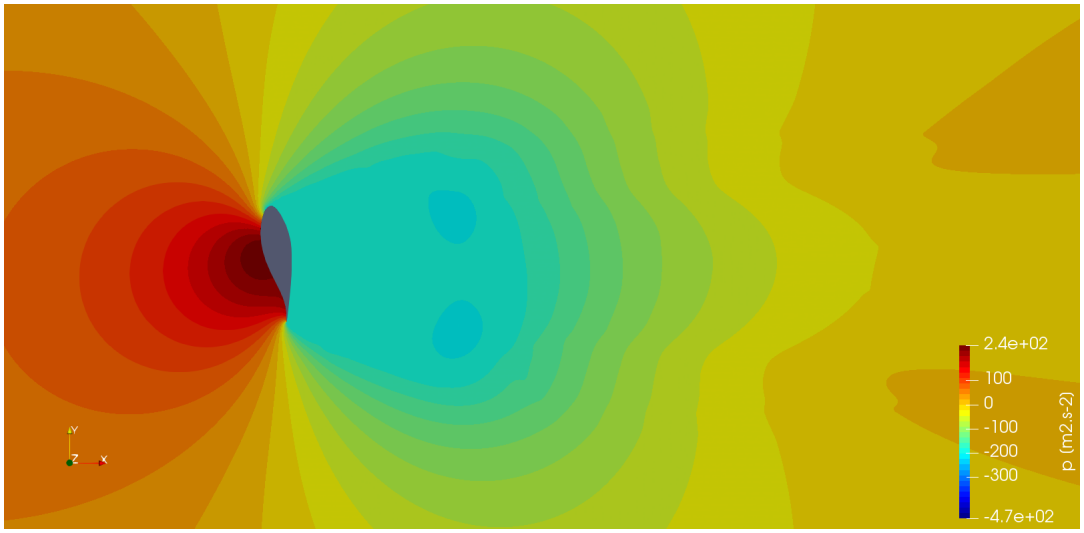

Figure 5. Pressure field at $t = 20\ s$

Regarding the pressure distribution (Fig. 5), phsically consistent results are observed. The pressure after contact with

the profile assumes several values that move away from the profile to the lower and upper boundary limits, returning to stables values as it flows to the outlet boundar condition, in accordance to the velocity field presented in Fig. 4.

The phenomenon presented, with the stagnation point located at the limits of the profile and also the large differences in pressure (approximately $400\frac{m^2}{s^2}$) between the front and back of the profile, point to the value of C_d of approximately 1.7 presented in Fig. 5.

3.3 Blade and Tower

For the cases of the blade with the presence of the tower, the results were obtained for the c_l and c_d presented in the Fig. 6. The values obtained represent the coefficients for the blade:

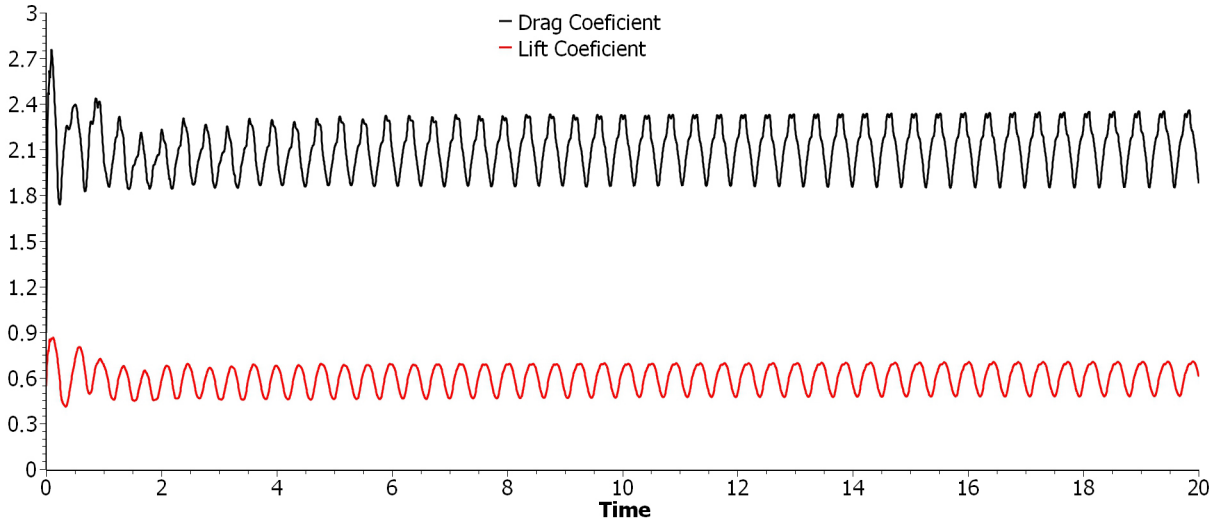

Figure 6. C_l and C_d Values Over Time

With the presence of the tower, it is possible to note a small increase in drag and lift values of the blade. The presence of the tower provides recirculation areas both in the front of the tower, after the flow deattaches from the blade, and in the rear of the tower, generating a decrease in pressure and consequently, changes in the values of lift and drag. The changes caused by recirculation, especially in the front of the tower, cause the velocity value to decrease between the two bodies, causing an increase in the coefficient, as shown in the Fig. 6. Similarly, the value of the drag coefficient was also slightly higher for this case, around 0.4 compared to the previous case.

Complementing the results, the Fast Fourier Transform (FFT) was performed to calculate the frequencies of oscillatory pattern present in the Fig. 6. Using the software *SciDAVis* (Standish, 2017), in which the result found was a frequency of $2Hz$.

Thus, the cylinder presented in the case, as fluid lines if closer to the body, greater lift due to all bodies, generating a lift maintenance value.

Unlike the blade-only case, the blade and tower experiment stabilizes much faster, around 0.7 second, generating converged results that were maintained until the end of the experiment. The region between the blade and the tower is a recirculation zone which has low velocity magnitude and low pressure values. The latter implies in higher lift coefficient when compared with the preavious case and could have led to faster stabilization of the flow.

When analyzing the case with the tower, it is possible to notice that some recirculation structure is formed during the passage by of the fluid the blade to the end of the tower. This structure ensures that the fluid does not separate from the body as seen in the Figure 7, and that it continues its trajectory after the blade profile towards the tower, resulting in a maintained recirculation behavior after the fluid passes through the tower, resulting in changes at the velocity and pressure values as presented in Figures 7 and 8.

Due to the behavior towards the tower, the speed values around the blade, in addition to fewer areas with a lower speed, guarantee a higher average lift coefficient if related only to the case of the blade, values that match the Figure 7.

4. Conclusion

When studying the effects of the blade profile with the tower, and performing a comparison of results, it was possible to observe that the effect of the presence of the tower alters the flow dynamics, changing from stable to oscillatory, with the alternating emission of vortices, a change noted in the difference between the cases.

A change in the values of drag and lift coefficients was noted in both cases, with larger values for the second case. The

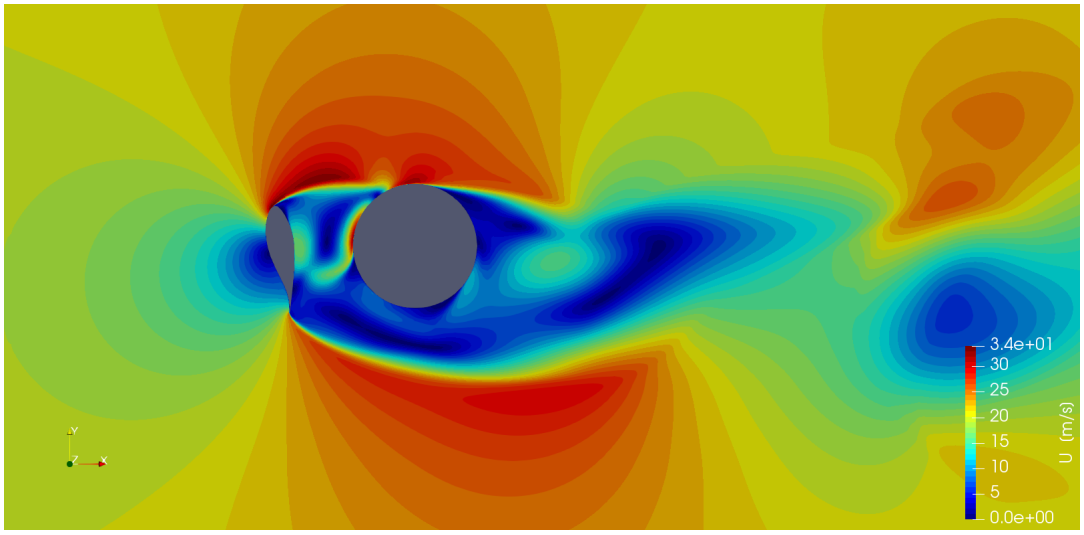

Figure 7. Simulation of velocity at the instant $t = 20$ s

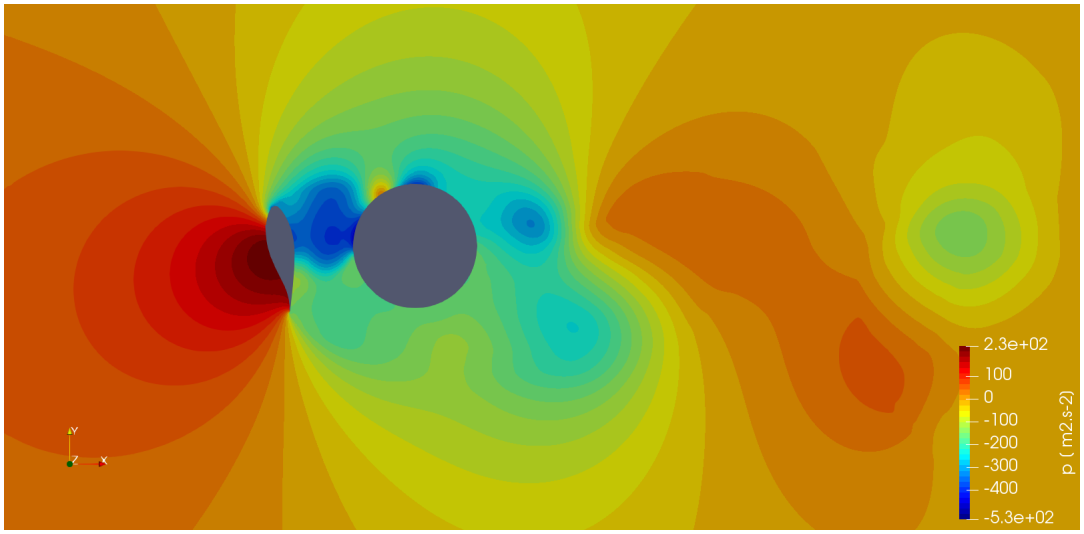

Figure 8. Simulation of pressure at the instant of time 20 s

aerodynamic coefficients obatiend in the present work are in good agreement with those in the literature [Jonkman et al. 2009].

The flow dynamics past the blade generates constant aeradynamic forces and a large stable wake. When the blade is positioned in front of the tower in tandem, the flow dynamics changes. The aerodnamic forces presents sinusoidal behavior and its averague value becomes about 25% higher than the previous case. Then, the interaction between the blade and the tower is not negligible.

5. REFERENCES

ABSOLAR, 2021. "Procura por energia solar no brasil aumentou mais de 50% na pandemia". https://www.absolar.org.br/noticia/procura-por-energia-solar-no-brasil-aumentou-mais-de-50-na-pandemia/.

Alfonsi, G., 2009. "Reynolds-averaged navier–stokes equations for turbulence modeling". *Applied Mechanics Reviews*, Vol. 62, No. 4.

Bojek, P., 2022. "Wind electricity - tracking report". https://www.iea.org/reports/wind-electricity. Acesso em: 01 de fevereiro 2022.

Brasileiro, G., 2021. "brasil sobe para a sexta posicao em ranking internacional de capacidade de energia eolica". https://www.gov.br/pt-br/noticias/energia-minerais-e-combustiveis/2022/04/brasil-sobe-para-a-sexta-posicao-em-ranking-internacional-de-capacidade-de-energia-eolica.

Celik, I.B., 2008. "Procedure for Estimation and Reporting of Uncertainty Due to Discretization in CFD Applications". *Journal of Fluids Engineering*, Vol. 130, No. 7. ISSN 0098-2202. doi:10.1115/1.2960953. URL https://doi.org/10.1115/1.2960953. 078001.

CFDOnline, L., 1998. "Turbulence properties, conversions & boundary estimations". https://www.cfd-online.com/Tools/turbulence.php.

EPE, 2021. "Matriz energética e elétrica". https://www.epe.gov.br/pt/abcdenergia/matriz-energetica-e-eletrica.

Ferziger, J.H., Perić, M. and Street, R.L., 2002. *Computational methods for fluid dynamics*, Vol. 3. Springer.

GWEC, 2021. "Global wind report 2021". https://gwec.net/global-wind-report-2021/.

Jonkman, B., 2016. "Du25_a17 conditions and data". https://github.com/old-NWTC/FAST/blob/master/CertTest/5MW_Baseline/Airfoils/DU25_A17.dat.

Jonkman, J., Butterfield, S., Musial, W. and Scott, G., 2009. "Definition of a 5-mw reference wind turbine for offshore system development". Technical report, National Renewable Energy Lab.(NREL), Golden, CO (United States).

Menter, F.R., 2003. "Ten years of industrial experience with the sst turbulence model". *Begell House, Inc*, Vol. 1, No. 4.

OpenCFD, L., 2018. "Backward facing step". https://www.openfoam.com/documentation/guides/latest/doc/verification-validation-turbulent-backward-facing-step.html.

Santoni, C., Carrasquillo, K., Arenas-Navarro, I. and Leonardi, S., 2017. "Effect of tower and nacelle on the flow past a wind turbine". *Wind Energy*, Vol. 20, No. 12, pp. 1927–1939. doi:https://doi.org/10.1002/we.2130.

Spalding, D.B., 1972. "A novel finite difference formulation for differential expressions involving both first and second derivatives". *International Journal for Numerical Methods in Engineering*, Vol. 4, No. 4, pp. 551–559. doi:10.1002/nme.1620040409. URL https://doi.org/10.1002%2Fnme.1620040409.

Standish, R., 2017. "What is scidavis?" https://scidavis.sourceforge.net/index.html.

6. RESPONSIBILITY NOTICE

The authors are solely responsible for the printed material included in this paper.